# 6. The effect of mechanical heterogeneity on diversification of deformation patterns - A modelling study with granular media

The evolution of a deformation system is driven by a multitude of both intrinsic and external parameters that may generate e.g., simple fold-and-thrust belts or plateau-style settings. We explore the distribution of mechanical properties on the development of different deformation patterns in granular analogue models monitored by high-resolution particle imaging velocimetry. This allows us to address the question which mechanical parameters may cause plateau-style deformation patterns. We show that plateau-style settings indeed only form when critical strength contrasts are present within the initial system, both laterally in the crust and with respect to its base. Threshold values for these parameters exist (at 20% lateral strength contrast and 35% basal contrast), which determine the style of the brittle analogue strain pattern: taper-like or plateau-style, without any transitional stages in between. Our models are able to reproduce the spatial and temporal distribution of strain accumulation as observed on the orogen scale of the Central Andean Altiplano. The driving factors that can explain the deformation pattern of this plateau orogen are still under debate. The fact, that the pattern of a complex natural system can be approximated by a simple model, implies that the pattern cannot be caused by only one parameter combination, and thus has no unique explanation. This ambiguity in turn precludes the possibility to conclude the responsible driving mechanisms from the respective strain patterns.

## 6.1. Introduction

A variety of parameters have been shown to influence the balance between plate boundary and buoyancy forces in controlling the evolution of orogens (e.g., McKenzie, 1969; Forsyth and Uyeda, 1975; Chapple and Tullis, 1977; Richardson et al., 1979; Dewey, 1980; Ranalli, 1987, more references in Sengör, 1990). More particularly, the resulting orogenic system and its internal deformation patterns depend on the impact of a. internal factors such as rheological heterogeneities within the plates (due to e.g., differential temperature, density properties, rock composition, inherited weaknesses, presence of fluids, etc.), crust-mantle interaction (decoupling, delamination, magmatism), and strain weakening; as well as on b. external factors like plate geometry, convergence kinematics, subduction angle, coupling along the plate interface, and climate.

The specific contribution of these individual parameters to and their role in the evolution of a particular deformation system is usually a matter of debate. Different strain accumulation patterns, e.g., plateau-style or wedge-like deformation (narrow single- or bivergent) etc., may grade into each other along-strike in spite of similar plate tectonic settings and also appear to exist in quite diverse tectonic settings. This becomes particularly clear when observing the lateral variability of the subduction-related Andes or of the collisional Himalayan-Alpine system. The spatial and temporal strain accumulation is extremely diverse and suggests complex system behaviour from interaction of a multitude of processes and properties.

Although a large number of controlling parameters have been proposed for the formation of the Andean Altiplano-Puna plateau (e.g., mantle-driven processes like delamination (e.g., Kay and Kay, 1993; Allmendinger et al., 1997); crustal channel flow (e.g., Wdowinski and Bock, 1994a;b; Yuan et al., 2000; Husson and Sempere, 2003); strength variations in the plates and their interface (e.g., Allmendinger and Gubbels, 1996; Lamb and Davis, 2003); climate (e.g., Lamb and Davis, 2003; Masek et al., 1994; Horton, 1999; Sobel et al., 2003); changes in plate/indenter geometry (e.g., Gephart, 1994; Tassara, 2005; Giese et al., 1999); and convergence kinematics (e.g., Pardo-Casas and Molnar, 1987; Somoza, 1998; Silver et al., 1998)); they so far do not account for the observed spatial and temporal evolution of the orogen-internal deformation pattern. With a correlation analysis of time series data of various processes

suggested for these deformation patterns for the Andean plateau, Oncken et al. (2006) have shown that only a special combination of parameters can explain the spatiotemporal strain distribution (namely differential feedback of trench infill, plate interface coupling, associated shortening transfer and slab rollback, as well as the position of inherited structures of crustal weakness). This strategy, however, hinges on the assumption that temporal and spatial correlation of coupled processes and strain accumulation provides a unique explanation for the observations. By the same token, numerical modelling of multiply coupled (mostly non-linear) processes often allow only the identification of one controlling mechanism, but not a distinct hierarchy of interdependent controlling mechanisms (cf. studies by e.g., Wdowinski and Bock, 1994a, b; Royden, 1996; Sobolev and Babeyko, 2005; Vietor and Oncken, 2005).

This ambiguity of interacting processes does not only preclude the understanding of what might stipulate complex system behaviour, which is neither easily identified from the rock record, nor in standard modelling approaches. The difficulty in demonstrating the uniqueness of parameter combinations also restrains the possibility to in turn use the resulting strain pattern of a structural system, leading to e.g., plateau-style or wedge-like deformation, to infer the key driving factors responsible for their formation.

In this paper we single out the individual role of mechanical heterogeneity, which is itself characterized by multiple factors, and system-atically investigate its contribution in controlling both the spatial distribution and timing of deformation. To address this question we perform analogue experiments in which we successively implement and change single mechanical properties and combinations thereof, so that initially simple systems become more complex. All experiments are monitored by particle imaging velocimetry permitting high resolution of resulting strain patterns in space and time (cf. Adam et al., 2004). This enables us 1) to explore and determine the effect, stability and uniqueness or non-uniqueness of mechanical heterogeneity driven by certain parameter combinations for their ability to develop plateau-style vs. wedge-like deformation systems, and 2) to contrast analogue strain patterns of model and nature caused by dissimilar parameter combinations.

## 6.2. Experimental design
### 6.2.1. Scaling analysis

The brittle crust is modelled by granular materials which show similar frictional-plastic behaviour as natural rocks, with a strain hardening phase until failure followed by a phase of strain weakening and localization (Byerlee, 1978; Mandl, 1988; Krantz, 1991; Marone, 1998; Schellart, 2000; Lohrmann et al., 2003). Thus, material is characterized by the coefficient of friction (internal and basal), cohesion, and density. Granular experiments are scaled to nature according to: $\sigma^* = C^* = \rho^* \lambda^* g^*$ (asterisk indicates ratios of model to nature, $\sigma$ is tectonic stress, C is cohesion, $\rho$ is density, $\lambda$ is the geometric length, and g is gravity) (e.g., Hubbert, 1937; Koyi, 1997; Schellart, 2000). The geometric scaling factor is given by: $\lambda^* = \rho_{nat} C_{mod} g_{nat} / \rho_{mod} C_{nat} g_{mod}$. Using typical density values for upper crustal rocks of about 2700 kg/m³ with cohesion being on the order of $<10^0$-$10^2$ MPa; and density values of about 1700 kg/m³ for the granular material, with cohesion being on the order of $10^0$ Pa-$10^2$ Pa at natural gravity of g = 9.81 m/s², our geometric scaling factor ranges between $10^{-4}$ to $10^{-8}$ (Table 6.1).

### 6.2.2. Materials and model construction

In granular set-ups, the strength of a material is mainly characterized by the coefficient of friction. We determine these coefficients using a ring shear device: shear stresses are measured for given normal loads and the appropriate values of coefficients of friction and cohesion for the peak, static-stable, and dynamic-stable frictions are thereafter determined by means of regression analysis (e.g., Lohrmann et al., 2003; Hampel et al., 2004). These are equivalent to the frictional strength until failure, the strength of fault reactivation, and the strength of actively deforming material respectively (Byerlee, 1978). Properties of materials used are summed up in Table 6.2.

The measurements yield absolute values with which we obtain the applied normal and shear stresses within the experiments by means of the Coulomb failure criterion: $\tau = c + \mu \sigma$. Thus for 0.018 m of model crust, a density of 1700 kg/m³ and natural gravity, a typical normal stress $\sigma_{mod}$ at the base of the analogue layer is 300 Pa. For a basal coefficient of friction of 0.5 with cohesion being negligible, the shear stress $\tau_{mod}$ at the base is 150 Pa, above which the material will fail.

In the following we will refer to the

Table 6.1. Scaling parameters

| Parameter | Equation | Nature | Model | Scaling factor |
|---|---|---|---|---|
| *Thickness upper crust* | $\sigma^* = \delta^* \, g^* \, L^*$ | 20 km | 1.8 cm | $L^* = 9.1 \times 10^{-7}$ |
| *Density* | $\delta_{mod}/\delta_{nat}$ | 2700 kg/m³ | 1700 kg/m³ | $\delta^* = 0.63$ |
| *Gravity* | g | 9.81 m s⁻² | 9.81 m s⁻² | $g^* = 1$ |
| *Cohesion* | C* | $10^0 - 10^2$ Pa | $10^{-4} - 10^{-8}$ Pa | |
| *Stress* | $\sigma^*$ | | | $\sigma^* = 5.74 \times 10^{-7}$ |

coefficients of friction for materials as the value of the dynamic-stable friction. Two simplifications have to be noted: we neglect cohesion, which is approximately one order of magnitude below the resulting stresses, and we neglect that the normal stress in the model is lower closer to the surface.

All materials are sieved into the model set-up. Vertical or inclined material boundaries are established by thin metal boards separating units during sieving, which are later removed. To obtain a plane surface, material is slightly compressed after sieving. If cohesion is to be kept low, barium sulphate must not be compressed at all. Finally, a marker grid of coloured sand is sieved on top of the experimental set-up with squares of 5 cm x 5 cm.

### 6.2.3. Dimensions of the experimental set-up

We carried out experiments with a scaling factor of 9.1 x 10⁻⁷ as well as with 4.55 x 10⁻⁷ for comparison. The experimental dimensions of 60 cm x 84.2 cm x 1.8 cm (width x length x height) respectively 30 cm x 42.1 cm x 0.9 cm equal 660 km x 925 km x 20 km in nature. We chose these values close to the natural analogue of the Central Andean plateau. The dimensions thus cover the area of the Altiplano plateau (17°-23°S) within the upper crust down to the decoupling horizon at 20 km depth (e.g., Yuan et al., 2000), adding the amount of shortening that has been accumulated (~265 km, e.g., Kley, 1999). The system is closed to the sides by glass panels to prohibit lateral extrusion of the material.

### 6.2.4. Monitoring technique

Most of the experiments were monitored by a special camera system using the technique of particle imaging velocimetry (PIV), which allows the quantification of instantaneous velocities and

displacements of particles (e.g., sand grains) during the experimental run (cf. Adam et al., 2004). One PIV camera is employed which monitors the 2D strain surface from above. The calibration of the camera before an experiment is used for the calculation of a mapping function, which accounts for image distortion. The calibration error for the experiments is on the order of 10⁻¹ pixel, which equals 0.038 mm, therefore being one order of magnitude smaller than the size of a single sand grain.

Sequential images are cross-correlated by the commercial software DaVis (e.g., adaptive multipass pattern cross-correlation employing Fast Fourier Transformation, for details refer to Adam et al., 2004). The observed velocity field can be decomposed into all components of the strain gradient tensor.

Additionally, digital images are sampled every second, which gives 24 images per centimeter of convergence at a motor speed of 2.5 cm/min.

### 6.3. Experimental results

We performed a series of more than 40 experiments (Appendix B), in which a piston compresses the initial set-up from one side (back wall) to the other (front wall) (cf. Fig. 6.1). The initial set-up generally consists of four structural units (termed unit 1, 2, 3, and 4) which are characterized by different material properties and therefore exhibit lateral strength contrasts (sand, glass beads, barium sulphate, salt, grains of rice pudding, grains of corn meal, starch, sugar).

Additional weak zones were introduced in units 1 and 3 (glass beads, salt, fine sand) as vertical columns (cf. Fig. 6.1). The position of the shear horizon is at the bottom of the experimental set-up, either "fixed" to the table (glass beads,

Table 6.2a. Coefficients of Internal Friction, Cohesion, and Density, as measured with the Ring shear apparatus

| Density (g/m³) | Peak friction $\mu_{peak}$ | Static-stable friction $\mu_{static}$ | Dynamic-stable friction $\mu_{dynamic}$ | Cohesion, Pa |
|---|---|---|---|---|
| *Sifted Dry Quartz Sand (Grain Size <0.63 mm)* | | | | |
| 1.73 | 0.70 | 0.60 | 0.54 | 140-90 |
| *Glass Beads (Grain Size <0.4 mm)* | | | | |
| 1.55 | 0.50 | 0.46 | 0.41 | 60-40 |
| *Barium Sulphate* | | | | |
| 1.26 | 0.82 | 0.79 | 0.76 | 460-360 |
| *Sifted Z-lights Ceramic Beads (Grain Size <0.4 mm)* | | | | |
| 0.65 | 0.48 | 0.46 | 0.43 | 60-35 |

| | *Corn Meal* | *Rice Pudding* | *Salt* | *Starch* | *Sugar* |
|---|---|---|---|---|---|
| Density (g/m³) | 0.71 | 0.89 | 1.49 | 0.59 | 1.01 |
| Friction (range) | 0.85-0.65 | 0.87-0.71 | 0.70-0.55 | 0.67-0.6 | 0.63 |

Table 6.2b. Coefficients of Basal Friction, Cohesion, and Density, as measured with the Ring shear apparatus

| Peak friction $\mu_{peak}$ | Static-stable friction $\mu_{static}$ | Dynamic-stable friction $\mu_{dynamic}$ | Cohesion, Pa |
|---|---|---|---|
| *Sifted Dry Quartz Sand (Grain Size <0.63 mm) vs. teflar foil* | | | |
| 0.32 | 0.23 | 0.23 | 103-160 |
| *Glass Beads (Grain Size <0.4 mm) vs. teflar foil* | | | |
| 0.19 | 0.11 | 0.11 | 150-200 |
| *Barium Sulphate vs. teflar foil* | | | |
| 0.41 | 0.27 | 0.26 | 90-160 |
| *Barium Sulphate vs. alcor foil* | | | |
| 0.53 | 0.5 | 0.5 | 74-33 |
| *Sifted Dry Quartz Sand (Grain Size <0.63 mm) vs. alcor foil* | | | |
| 0.36 | - | 0.30 | - |
| *Sifted Dry Quartz Sand (Grain Size <0.63 mm) vs. sand paper* | | | |
| 0.63 | 0.58 | 0.55 | 66-62 |
| *Glass Beads (Grain Size <0.4 mm) vs. sand paper* | | | |
| 0.5 | 0.49 | 0.46 | 21-1 |

fine sand, Teflon foil or alcor foil) on which the experiments were run, or "loose" with additional material (glass beads, fine sand, salt) between the units and the fixed foil on the table. Depending on the implemented parameter characteristics and combinations, five different deformation systems evolve, which we describe in order of increasing complexity. All five types generally follow either a "wedge-like" or "plateau-style" deformation. A summary of the initial set-up, structural evolution and final results are summarized for each experiment in Appendix B.

### 6.3.1. Single "wedge-like" setting, (Fig. 6.1a)

The taper configuration represents the classical wedge (Fig. 6.1a), which increases in taper angle and sheds sediments over its slope with continuing compression until a certain point when it becomes stable. All structural units (1-4) are involved in its formation.

### 6.3.2. Bivergent "wedge-like" setting, (Fig. 6.1b)

This set-up produces a peak ridge in the center (unit 2) which has symmetric slopes verging to both sides (Fig. 6.1b). Sediments shed down these slopes on both sides.

### 6.3.3. Low-angle "wedge-like" setting, (Fig. 6.1c)

One peak ridge develops close to the moving piston in unit 1, followed by uplift of the area adjacent to this peak ridge (unit 2), which itself is only little deformed. This area has the same elevation as the peak ridge. Thrusts form subsequently in units 3 and 4 (Fig. 6.1c). The resulting taper has a rather low angle, as most units have the same elevation.

### 6.3.4. High "plateau-style" setting, (Fig. 6.1d)

This setting is similar to c), but after the first peak ridge has formed in unit 1, another peak ridge develops in unit 3, adjacent to unit 2. Unit 2 has been uplifted to approximately the same elevation as both peak ridges, but in contrast, has not been highly deformed. Again, additional thrusts develop further away from the piston in unit 4 (Fig. 6.1d).

### 6.3.5. "Plateau-style" setting, (Fig. 6.1e)

This deformation system (Fig. 6.1e) is characterized by the development of two peak ridges (units 1 and 3), both adjacent to unit 2, which itself forms a plateau area. The plateau area lies at a higher elevation than the initial surface, but remains at a lower elevation than the peak ridges. The peak ridges shed sediments on top of the plateau surface. Thrusts develop in unit 4 as soon as deformation in both peak ridges and the plateau area becomes inactive.

### 6.4. Parameter control

The five described settings develop in response to two main controlling parameters: a. the basal detachment, and b. the lateral strength variation between structural units. Both parameters can be expressed in terms of strength contrasts, which yield dimensionless ratios: a. "basal contrast": basal friction (with respect to unit 2)/ internal friction (of unit 2), and b. "lateral contrast": internal friction of stronger unit/ internal friction of adjacent weaker unit. In some experiments, weak zones are implemented in units 1 and 3, which allow further variation with respect to the units' strength.

### 6.4.1. Basal strength contrasts

The basal detachment is positioned beneath the set-up as a foil fixed to the table, which is characterized by the basal coefficient μ of the foil with respect to the material above (we use unit 2 as reference material, here baryte) which ranges from 0.26 for teflar foil, 0.45 for alcor foil, 0.55 for glass bead foil, up to 0.65 for sand paper. In some experiments, an additional material layer of sand, salt, or glass beads is implemented between the foil and the set-up (with internal coefficients of friction of 0.54, 0.55, and 0.41 respectively). The respective value for basal friction depends on the thickness of the additional layer. If it is ~3 mm or thicker, the effect of the foil becomes minimal and we take the internal value of the material. If the thickness is lower, we take the mean value of both the basal friction of the foil and the internal friction of the additional material.

The basal strength contrast is the ratio between the mean basal friction with respect to the material of unit 2 and the internal friction coefficient of unit 2. This ratio has a threshold value close to 0.67, which determines if the deformational style is wedge-like (>0.67; a, b, c) or plateau-like (<0.67; d, e) (Fig. 6.2).

The presence and properties of the additional layer determines the type of plateau-style setting. Setting d) requires additional material beneath the set-up, as it supports the uplift of a plateau surface, whereas type e) only develops, when no additional material is present. Setting c) of the wedge-like systems also requires additional material below the set-up, but with a higher basal friction than d).

We further have to note that in some experiments we varied the properties of the basal horizon along-strike (Appendix B, Exp. 35, 43, 45). It then depends on the position of the piston (i.e., amount of convergence), which of the basal properties are effective. Thus, the basal
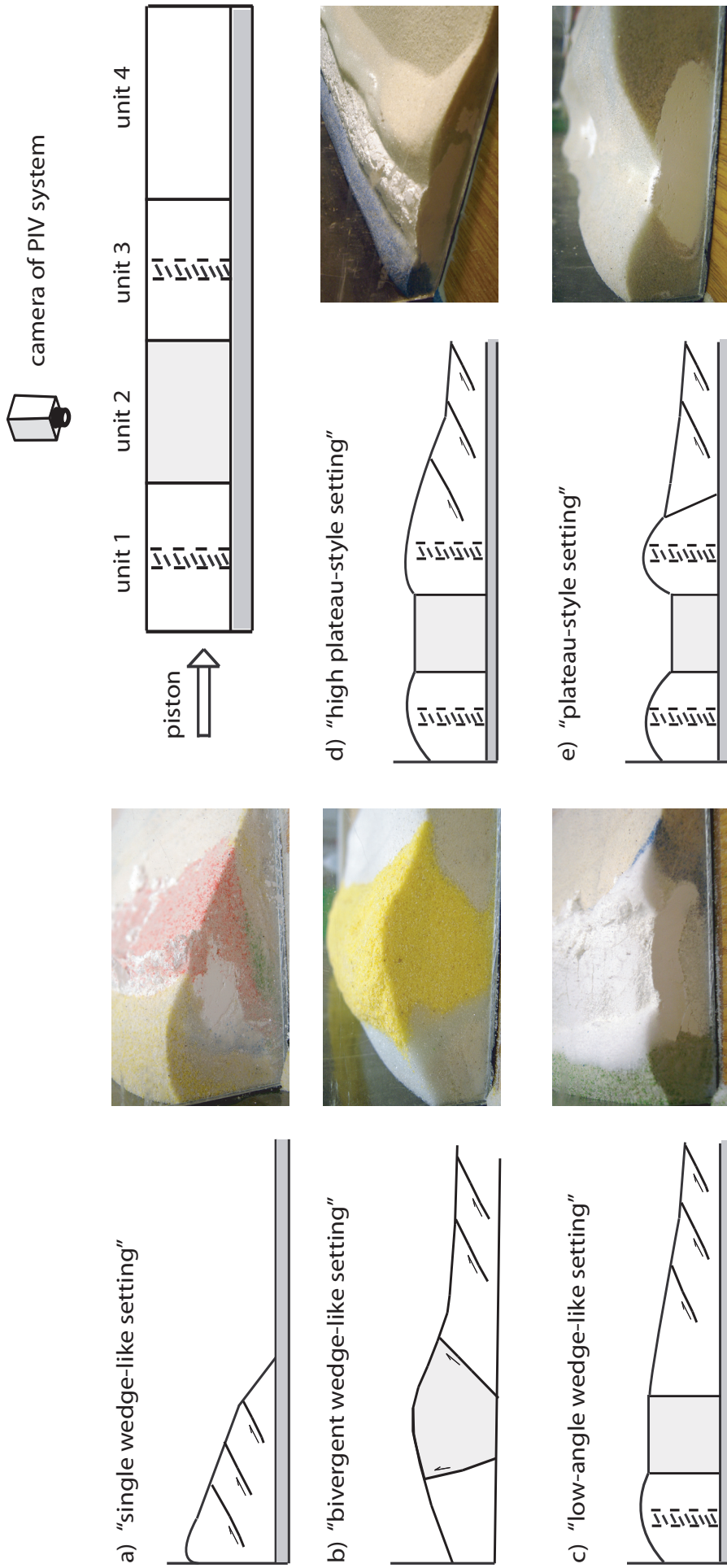
Fig. 6.1: The initial set-up (upper right) results in settings a. to e. depending on the mechanical properties of the system. The five types can be grouped into two main deformational types: wedge-like (on the left) and plateau-like (on the right). Threshold values exist for both the basal and the lateral strength contrasts determining if either the one type or the other evolves. For each of the settings a sketch and a photograph of the final set-up are shown. Further explanations in-text.

effect on the deformation system changes over time, and the plateau-style setting might become taper-like at a later stage.

### 6.4.2. Lateral strength contrasts

Lateral strength contrasts are defined as the ratio of the internal friction coefficient of the strongest unit (unit 2) and the mean internal friction of the weaker unit adjacent to the strong unit (units 1 and 3). If no lateral variation is present, the ratio is 1. It becomes greater than 1 with increasing lateral strength contrast, i.e., the strong unit becomes stronger or the weak unit weaker. Internal friction coefficients of the materials used for the four structural units range from 0.38 (glass beads 40-70 μm) to 0.76 (baryte). In some experiments, we put additional weakness zones within units 1 and 3

to localize deformation in these units and to initiate their uplift. The value for the mean internal friction is calculated depending on the percentage of the widths of the weakness zones.

Again, a threshold value for the minimum contrast exists laterally, that has to be overcome to develop a plateau-style rather than a taper-like setting (Fig. 6.2). When the contrast is 1 or slightly higher, the resulting system will be taper-like (a.). If the ratio is about 1.2 or higher, a taper-like setting (both a. and c.) only develops when the basal contrast is higher than ~0.35 at the same time. Else, the setting will be plateau-like (Fig. 6.2).

This is only true for materials that have similar densities. For instance, when the material in unit 2 has a much lower density than materials of adjacent units 1 and 3 (e.g., ~600-900 kg/m³
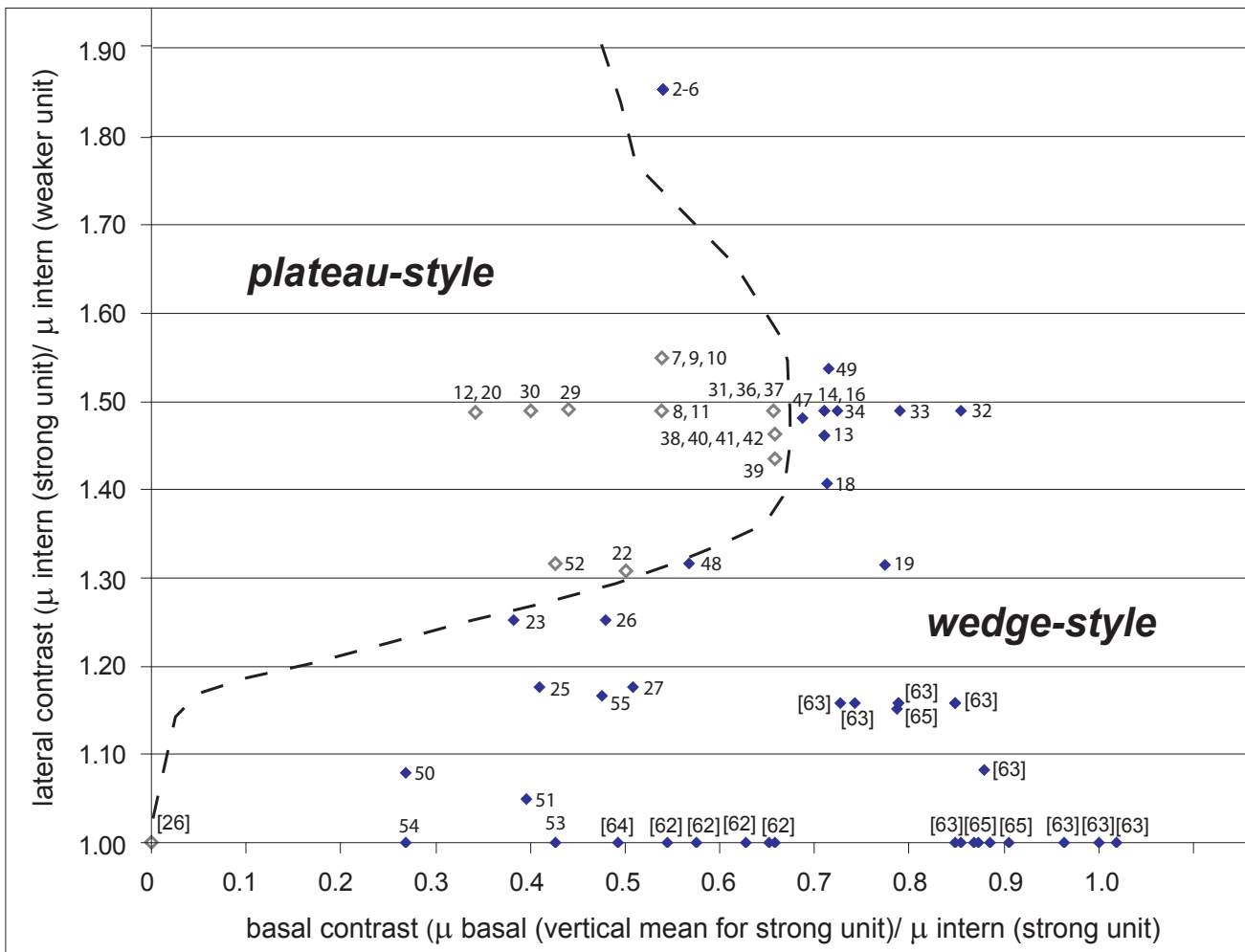


*Fig. 6.2: This plot shows the dependence of the deformation style (taper- or plateau-like) on the basal strength contrast (x-axis) and the lateral strength contrast (y-axis) within the system. The basal contrast is defined as the ratio of the basal coefficient of friction (with respect to the strongest unit) and the internal friction coefficient of the strongest unit. The lateral contrast is defined by the ratio of the internal friction of the strongest unit and the internal friction of the weaker material adjacent to the strong unit. Both ratios are dimensionless. Plateau-style settings plot as outlined diamonds (including settings d. and e.), taper-like settings plot as solid diamonds (settings a., b., and c.). The dashed line separates the two fields. The numbers indicate the experiment numbers summarized in Appendix B. Numbers in brackets indicate the following references: [26] Vietor, pers.comm., 2007; [62] Schreurs et al., 2006; [63] Lohrmann, 2002; [64] Marques and Cobbold, 2002; [65] Hoth, 2005. Values for each of the points are summarized in Table 6.3. Further explanation in-text.*

vs. ~1500-1800 kg/m³), the resulting setting is bivergent (b), as material is squeezed upwards during compression.

### 6.4.3. Shape of the indenting piston

If the curvature angle was low (<20°) and already attained before convergence, the effect of the bent indenter is not very strong compared to the boundary effect of side wall friction (cf. Schreurs et al., 2006). If the indenter is initially straight and highly gains in curvature during convergence (up to >45°), the material is moving parallel to the direction of convergence only in the center point of the indenter and has a higher translational component towards the sides.

### 6.4.4. Effect of strong lithosphere on the backside of the orogen

We modelled a strong lithospheric block or mass by placing a wooden plate with a slope at the back of the experimental set-up, so that material of the fold-and-thrust belt can thrust on top of it. For angles of less than 10° there is no distinction within the general setting. If the angle was higher, material would not overcome the boundary to thrust on top, but rather piles up in front.

### 6.4.5. Internal geometries and symmetries

When the structural units are wider, more thrusts can take up more bulk shortening. If the crust is thicker, the spacing of thrusts will increase, and the peak ridges can uplift higher. The additional weakness zones in units 1 and 3 allow the localization and uplift initiation of the peak ridges, when they make up at least 6% or more of the initial width of the structural unit. If weak zones are wider than necessary, more material is squeezed or thrust, which subsequently falls down the slopes onto the plateau.

If the strength contrasts from units 1 and 3 to unit 2 are not the same on either side, both peak ridges form, but the plateau surface in between has a dip towards the peak ridge with the lower strength, producing an asymmetric setting.

We also tested vertical material boundaries vs. boundaries at an angle, for which we did not see any differences in outcome.

### 6.5. PIV monitoring of plateau-style settings
### 6.5.1. Plateau without erosion

We monitored the plateau-style setting e) with the PIV technique described above to obtain the displacement field for every single time step (one image every second, convergence rate: 2.5 cm/min, about 40 cm of total convergence). Figure 6.3 shows a PIV image from the surface of the experiment showing incremental strain in the direction of convergence ($E_{xx}$ in %). It depicts
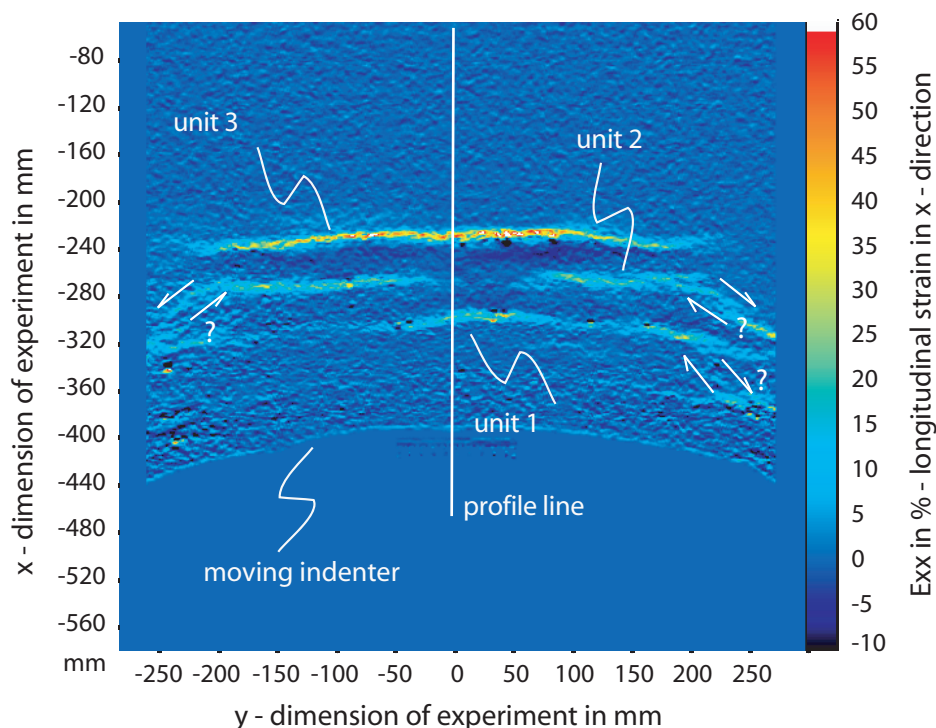


*Fig. 6.3: PIV strain image of experimental surface after 12 cm of convergence. Lighter colours indicate zones of incremental strain in the x-direction (direction of convergence); here three thrusts are currently active in three different units. Also visible are potential strike-slip components close to the sides, and the outline of the indenter. The white vertical line marks the position of the profile shown in Figure 6.4a and Figure 6.5a.*

localized deformation along the two peak ridges as well as one thrust within the plateau area. The curved indenter might have caused transpressional structures close to the sides of the set-up, but as these structures are not well defined, they probably result from side wall friction (cf. Schreurs et al., 2006).

We extract the strain data along one profile crossing the surface area for each image to obtain a time series of strain accumulation in space (Fig. 6.4a). Structures develop first in the upper left and move down to the lower right, as time increases from top to bottom and convergence is from left to right. The black areas represent zones of high strain accumulation. First, the peak ridge close to the piston develops with three thrusts (marked 1 to 3), representing the initial uplift within the weak zone. The white colour to the left of the structure indicates avalanches from the peak ridge. In this

initial phase, avalanches occur away from the plateau interior towards the indenter. The fourth thrust of peak ridge 1 is coevally active with the initiation of thrusting within the plateau area, which is directed towards the foreland (marked 4 and 5).

While the second thrust within the plateau is still active, and uplift of the first peak ridge is ongoing, the uplift of the second peak ridge starts (5), again within the weak zone. Avalanches become stronger (from both thrusts 5 and 6) and thrusting within the plateau dies out. Unlike the initial phase, avalanches from both peak ridges are directed towards the plateau interior. As directions of avalanches typically correlate with the direction of thrust motion, we gain information on the internal structures from surface data and are able to reconstruct a cross section (Fig. 6.4b). Here, the avalanches indicate that the vergence of thrusts within the first peak ridge has changed
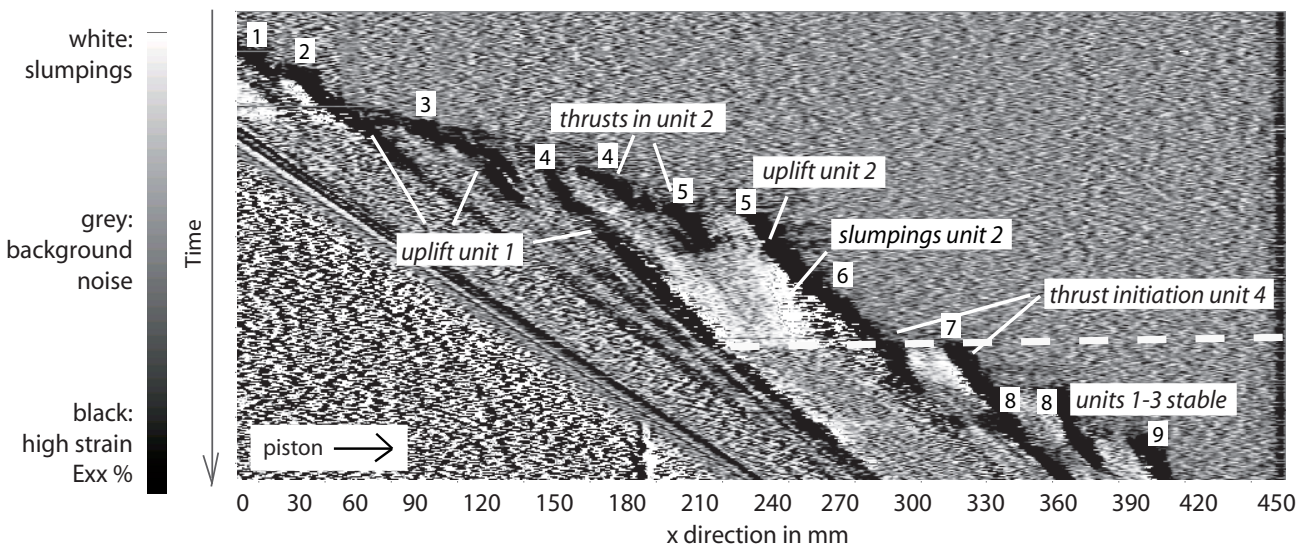


*Fig. 6.4a (top) + b (bottom): a) Strain data along profile through center of experiment "plateau-style setting without erosion" (cf. Fig. 6.3) for all time increments. Active thrusts are black, avalanches are white, and background noise is grey. Active thrusts are chronologically numbered, the structural units are also marked. Further explanation in-text; b) Sketch of cross section of the finite (top) and balanced (bottom) plateau-style setting. Thrusts are chronologically numbered as in a).*
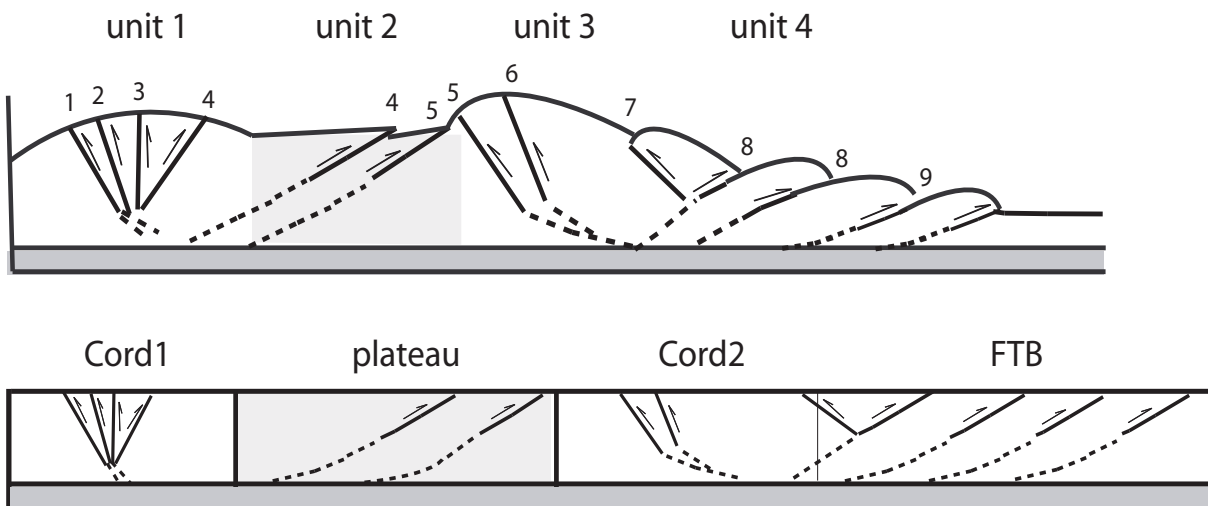
towards the foreland (4), and backthrusts are no longer active (1 to 3). Backthrusts are only active within the second peak ridge (5, 6).

The white dashed line in Figure 6.4a marks the time increment when the first thrust of the wedge-like part (unit 4) becomes active, coeval with the halt of avalanches from both peak ridges, which means that deformation is no longer active. Thus, plateau-style deformation stops, and wedge-like deformation becomes dominant in unit 4. Avalanches of thrust 7 towards the piston die out and thrusts with opposite vergence (to the foreland) become active (8). From that point on, thrusts propagate towards the front wall.

### 6.5.2. Plateau with erosion

We eroded along peak ridge 1 close to the piston for the first time after 4 cm of convergence, when it had already attained some elevation and then every 4 cm until peak ridge 2 started to develop, which we eroded every 4 cm from 29 cm onwards (constant erosion approach). The combined strain profile through time in Figure 6.5a shows that the relative chronology of activity within the units is the same as in Figure 6.4a. However, the number of faults is less in units 1 and 3 (three instead of four thrusts in unit 1, and one instead of three in unit 3), but higher in the plateau area (three instead of two). Avalanches are smaller as sediment supply is less, but they are of longer duration.

Each of the thrusts in the peak ridges and the plateau region is active for a longer period of time, with faults being reactivated (e.g., in the plateau region). In contrast, faults within the
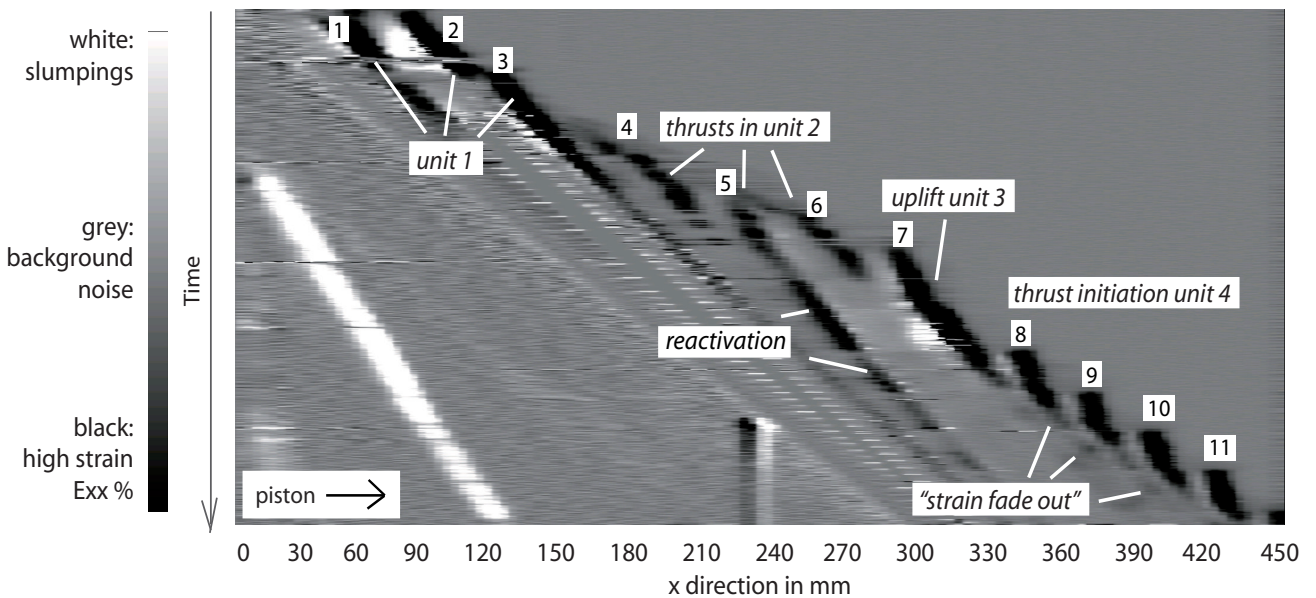


*Fig. 6.5a (top) + b (bottom): a) Strain data along profile through center of experiment "plateau-style setting with erosion" (cf. Fig. 6.3) for all time increments. These profiles are taken from an experiment in which material of unit 1 is eroded every 4 cm of convergence up to 29 cm of shortening, after which unit 3 is eroded. Active thrusts are black, avalanches are white, and background noise is grey. Thrusts are numbered according to their start of activity. Further explanation in-text; b) Sketch of cross section of the finite (top) and balanced (bottom) plateau-style setting with erosion. Thrusts are chronologically numbered as in a).*
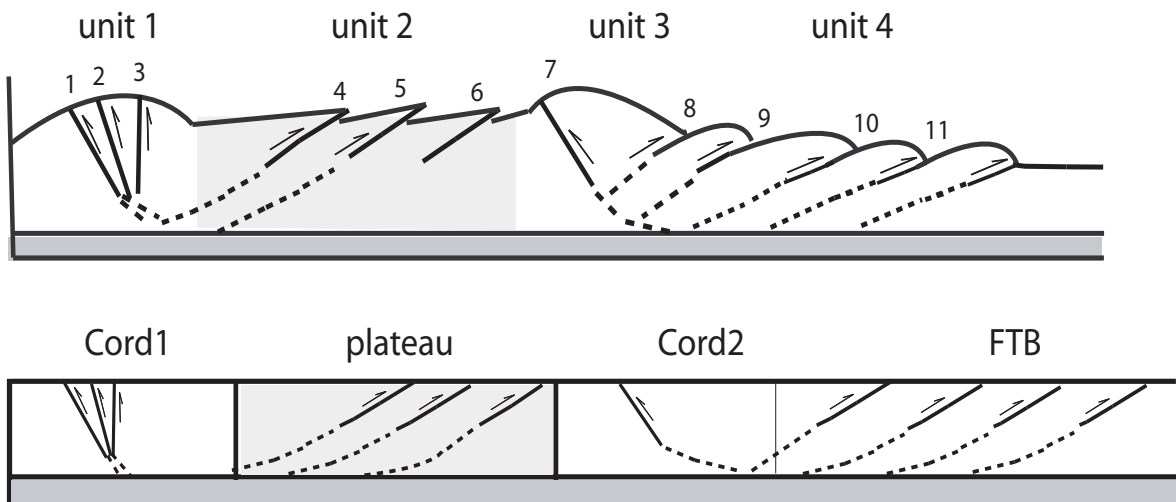
wedge-like part (unit 4) accumulate strain for a shorter period of time. Towards the end of a thrust's activity, strain accumulation "fades out" to almost zero, which is indicated by the faint black tail (Fig. 6.5a). The direction of avalanches indicates that faults in the peak ridges are all backthrusts (Fig. 6.5b).

### 6.6. Discussion
#### 6.6.1. Internal parameter control

Despite being a rather simple model of the upper crust, the granular set-up is able to show that certain parameters in combination are responsible for the evolution of two prominent types of strain accumulation. These parameters comprise two internal parameters that are coupled to each other: basal strength contrasts (including basal detachments) and lateral strength contrasts (including inherited structures). Thus, rheological properties of the system causing mechanical heterogeneity are first order factors controlling the style of strain accumulation. Figure 6.2 shows that two domains exist: one for plateau-like patterns and one for taper-like deformation (including both single- and bivergent settings), which can be separated from each other by a sharp line. This means that no gradual transitions exist from one type to the other, but that critical threshold values are present for both the lateral and the basal strength contrast, which determine if either the one or the other deformational setting develops.

The threshold value for lateral strength contrasts between adjacent units has to be higher than ~1.2 (or ~20% lateral strength contrast) for the formation of a plateau-style setting, which converges towards 1 when the basal contrast approaches 0 (no frictional coupling at the base). Numerical experiments have shown that as soon as the slightest basal friction is present (Vietor, pers. comm. 2007), deformation will be in a wedge-like rather than a plateau-style fashion, irrespective of lateral strength contrasts. Therefore we assume that the lower end of the line separating the two deformational settings will draw near to this point at 0 (basal contrast) and 1 (lateral contrast) (Fig. 6.2). At the same time, this means that without the lateral strength contrast the resulting strain pattern will always be wedge-like for any basal contrast >0.

The threshold value for the basal contrast is ~0.67 (or ~35% basal strength contrast) beyond which the strain pattern will be wedge-

like, irrespective of lateral strength contrasts. If the value for the basal strength contrast is lower than the respective threshold value, the style of deformation will be plateau-like independent from any increase of the lateral strength contrast beyond the above mentioned value (~1.2). However, some experiments (1-6, Fig. 6.2) indicate that if the lateral strength contrast will be very high (more than 50%) the plateau-style settings only develop when we again decrease the basal contrast.

Certainly, these values might shift depending on the aspect ratios of the initial system. This means, that with increased thickness of the upper crustal layer (but constant width of the units), the normal stress increases, and a higher shear stress or a lower basal friction is required for yielding (according to the Mohr-Coulomb criterion). The contrary is true for higher lateral widths with the same thickness, as the normal force is lower (i.e., the force acts on a bigger surface), and therefore the yield strength can be overcome at lower shear stresses or comparably higher basal friction. With respect to this issue, the line separating both fields might shift slightly to the left or right depending on the scaling ratio. However, the two different scaling ratios tested in our experiments have very similar threshold values.

We also conclude that plateau-style settings require more mechanical heterogeneity (complexity), as they develop only when both the basal and the lateral strength contrasts exist. In contrast, taper- or wedge-like systems already develop when only a basal contrast is present, but no lateral variation.

We can show that a hierarchy exists for all parameters. The controlling first order factors are basal and lateral strength contrasts. But, as taper-like settings already develop with only the basal contrast and do not necessarily require a lateral strength contrast, we interpret the basal contrast to be more important than the lateral contrast. The other tested internal parameters did not have any influence on the resulting deformation style, and are therefore only second order factors.

#### 6.6.2. Effect of external parameters

In our experiments, the external parameters such as shape of the indenter, the effect of a backstop or erosion merely cause a system to react to imposed changes, which can go as far as putting a system into a supercritical or subcritical state.

Table 6.3. Basal and internal friction coefficients used for the calculation of values for basal and lateral contrasts (cf. Figure 6.2)

| No | Basal friction (foil) | Basal friction (additional material) | Basal friction (average) | Internal friction (strong unit) | Internal friction (weak unit) | Basal contrast | Lateral contrast | Deformation type |
|---|---|---|---|---|---|---|---|---|
| 02 | | 0.41 | | 0.76 | 0.41 | 0.54 | 1.85 | a) |
| 03 | | 0.41 | | 0.76 | 0.41 | 0.54 | 1.85 | a) |
| 04 | | 0.41 | | 0.76 | 0.41 | 0.54 | 1.85 | a) |
| 05 | | 0.41 | | 0.76 | 0.41 | 0.54 | 1.85 | a) |
| 06 | | 0.41 | | 0.76 | 0.41 | 0.54 | 1.85 | a) |
| 07 | | 0.41 | | 0.76 | 0.49 | 0.54 | 1.55 | d) |
| 08 | | 0.41 | | 0.76 | 0.51 | 0.54 | 1.49 | d) |
| 09 | | 0.41 | | 0.76 | 0.49 | 0.54 | 1.55 | d) |
| 10 | | 0.41 | | 0.76 | 0.49 | 0.54 | 1.55 | d) |
| 11 | | 0.41 | | 0.76 | 0.51 | 0.54 | 1.49 | d) |
| 12 | 0.26 | | | 0.76 | 0.51 | 0.34 | 1.49 | e) |
| 13 | | 0.54 | | 0.76 | 0.52 | 0.71 | 1.46 | c) |
| 14 | | 0.54 | | 0.76 | 0.51 | 0.71 | 1.49 | a) |
| 15 | | 0.54 | viscous | 0.76 | 0.52 | – | 1.46 | e) |
| 16 | | | | 0.76 | 0.51 | 0.71 | 1.49 | c) |
| 18 | | 0.55 | | 0.76 | 0.54 | 0.72 | 1.41 | c) |
| 19 | | 0.55 | | 0.71 | 0.54 | 0.77 | 1.31 | b) |
| 20 | 0.26 | 0.5 | | 0.76 | 0.51 | 0.34 | 1.49 | e) |
| 22 | 0.26 | | 0.38 | 0.76 | 0.58 | 0.5 | 1.31 | d) |
| 23 | 0.25 | | | 0.65 | 0.52 | 0.38 | 1.25 | b) |
| 25 | 0.25 | | | 0.6 | 0.51 | 0.41 | 1.18 | b) |
| 26 | 0.35 | 0.41 | 0.305 | 0.65 | 0.52 | 0.47 | 1.25 | b) |
| 27 | 0.35 | 0.41 | 0.305 | 0.5 | 0.51 | 0.51 | 1.18 | b) |
| 29 | 0.36 | 0.41 | 0.335 | 0.76 | 0.51 | 0.24 | 1.49 | d) |
| 30 | 0.3 | | | 0.76 | 0.51 | 0.40 | 1.49 | e) |
| 31 | 0.5 | | | 0.76 | 0.51 | 0.66 | 1.49 | e) |
| 32 | 0.65 | | | 0.76 | 0.51 | 0.86 | 1.49 | a) |
| 33 | 0.6 | | | 0.76 | 0.51 | 0.79 | 1.49 | a) |
| 34 | 0.55 | | | 0.76 | 0.51 | 0.72 | 1.49 | a) |
| 35 | 0.5/0.65 | | 0.66/0.86 | 0.76 | 0.51 | 0.66/0.86 | 1.49 | e), then a) |
| 36 | 0.5 | | | 0.76 | 0.51 | 0.66 | 1.49 | e) |
| 37 | 0.5 | | | 0.76 | 0.51 | 0.66 | 1.49 | e) |
| 38 | 0.5 | | | 0.76 | 0.52 | 0.66 | 1.46 | e) |
| 39 | 0.5 | | | 0.76 | 0.53 | 0.66 | 1.43 | e) |
| 40 | 0.5 | | | 0.76 | 0.52 | 0.66 | 1.46 | e) |
| 41 | 0.5 | | | 0.76 | 0.52 | 0.66 | 1.46 | e) |
| 42 | 0.5 | | | 0.76 | 0.52 | 0.66 | 1.46 | e) |
| 43 | 0.5/0.65 | | 0.66/0.86 | 0.76 | 0.52 | 0.66/0.86 | 1.46 | e), then a) |
| 44 | 0.5 | | | 0.76 | 0.52 | 0.66 | 1.46 | e) |
| 47 | 0.55 | | | 0.8 | 0.54 | 0.69 | 1.48 | a) |
| 48 | 0.3 | | | 0.54 | 0.41 | 0.56 | 1.32 | a) |
| 49 | 0.45 | | | 0.63 | 0.41 | 0.71 | 1.54 | b) |
| 50 | 0.11 | | | 0.41 | 0.38 | 0.27 | 1.08 | a) |
| 51 | 0.17 | | | 0.43 | 0.41 | 0.4 | 1.05 | b) |
| 52 | 0.23 | | | 0.54 | 0.41 | 0.43 | 1.32 | d) |
| 53 | 0.23 | | | 0.54 | 0.54 | 0.43 | 1 | a) |
| 54 | 0.11 | | | 0.41 | 0.41 | 0.27 | | a) |
| 55 | 0.3 | | | 0.63 | 0.54 | 0.48 | 1.17 | b) |
| [62] | 0.3 | 0.37 | 0.335 | 0.67 | 0.67 | 0.54 | | a) |
| [62] | 0.3 | 0.47 | 0.385 | 0.67 | 0.67 | 0.57 | | a) |
| [62] | 0.3 | 0.49 | 0.395 | 0.63 | 0.63 | 0.66 | | a) |
| [62] | 0.3 | 0.41 | 0.355 | 0.54 | 0.54 | 0.66 | | a) |

Such a parameter influence becomes most obvious when comparing a system that has undergone erosion to one that has not been eroded. In general, erosion prolongs the activity of each thrust as well as the general uplift activity within the plateau-like part of the system, and therefore avalanches take place for a longer time than without erosion, but are small as sediment supply is scarce. Strain seems to be more localized in space and along fewer faults in the experiment with erosion, as thrusts are reactivated more often. Also, the deformation transfer from the stable plateau-style system (units 1-3) to the "external" wedge-like part (unit 4) can only be clearly observed without erosion. This is due to the fact, that the system does not become critical under the continued influence of erosion, an influence to which the system has to react and to adjust. Models by Babeyko et al. (2006) show that the effect of low to moderate erosion rates are negligible, but that high erosion rates at the plateau margin result in strain weakening of the lithosphere, which in turn leads to an increase of shortening rate within the plateau.

In general we can say that the spatiotemporal strain partitioning mode on the orogen scale resulting from internal parameter control cannot be affected by external parameters. Only minor changes on a sub-orogen scale can occur both in time (prolonging deformation activity in one unit) and space (number of faults) with some external parameters (e.g., erosion).

### 6.6.3. Limitations of the set-up

We are able to show the importance of the effect of basal contrasts by means of varying the frictional properties analogue to mechanical properties of natural systems. However, modelling only the brittle upper crust and decoupling it from a stiff base implies an important limiting boundary condition, unless layers down to the asthenosphere are incorporated. Also, isostatic effects (e.g., buoyancy) are not taken into account. We assume that isostatic effects have an influence on the general crustal thickness, the topographic elevation, and also on the spatiotemporal pattern of strain accumulation because of the different role of body forces. But as we suspect that isostatic effects would vary locally in response to rheological and therefore mechanical heterogeneities, it would further support our conclusion, that mechanical heterogeneities are first order factors in determining

Table 6.3. A description of each of the experiments (with corresponding numbers) is found in Appendix B. Values are determined on the base of basal and internal coefficients of friction (Table 6.2 a+b). In some cases the basal friction of only the foil or only the material was used, in other cases we used the average of both of these values (more details in-text). The values from Schreurs et al., 2006 [62], Lohrmann, 2002 [63], Marques and Cobbold, 2002 [64], and Hoth, 2005 [65] were partly reinterpreted to fit the value format that is used for Figure 6.2. Values from three experiments were not used in the plot, either because the material strength cannot be expressed in terms of friction coefficients (Exp. 15), or because the resulting deformation type changes during the experiment, as the basal friction varies laterally (Exp. 35, 44) (more details in-text).

the resulting strain pattern and deformation style.

### 6.7. Application to the Central Andean plateau

Today's Central Andes (17-23°S) have developed since the Paleogene due to the convergence between the Nazca plate and South America. From west to east they comprise four main structural units: the Pre- and Western Cordillera, the Altiplano plateau, the Eastern Cordillera, and the Subandean fold-and-thrust belt (Fig. 6.6). The plateau itself has an average elevation of 4000 m and is bounded by two Cordilleras with average elevations of about 5000 m (Lamb et al., 1997). The Pre- and Western Cordillera represent a former and the recent magmatic arc, and formed since about 46 Ma ago involving <2 % of shortening; the Eastern Cordillera developed as a fold-and-thrust belt since c. 40 Ma with some 30% of shortening, and the plateau has developed as an intramontane basin that has undergone deformation (<20% shortening) since 30 Ma (Elger et al., 2005). Deformation became inactive in all of these units c. 7-10 Ma ago, when active deformation was transferred to the Subandean fold-and-thrust belt (Allmendinger and Gubbels, 1996: "simple shear"

mode for the Altiplano), that has accumulated most of the shortening (~100 km, or 50%).

Both Cordilleras formed at positions of inherited structures: a Permoliassic rift in the Eastern Cordillera (Sempere et al., 2002), and the magmatic arc in the Western Cordillera (Oncken et al., 2006), which act as zones of weakness. A low-velocity zone at a depth of 20 km as imaged in seismic sections can be interpreted as a zone of partial melt possibly decoupling deformation of the upper crust from that of the lower crust (Yuan et al., 2000), which has probably developed since about 30 Ma ago (Babeyko et al., 2002). This horizon possibly extends to the east connecting with the detachment of the Subandean fold-and-thrust belt, which is located in Ordovician shales (Kley et al., 1996), and might be underthrust by the cold Brazilian Shield (Babeyko and Sobolev, 2005). To the west of the Western Cordillera, the little internally deformed forearc might have acted as a "pseudo-indenter" pushing into the comparably weaker orogen during subduction (Victor et al., 2004; Tassara, 2005). Thus the orogen would have been squeezed between two comparably stronger units: the forearc and the Brazilian Shield.

The orogen exhibits a symmetric oroclinal bend (Gephart, 1994) with its symmetry axis coinciding with the present direction of plate convergence. Both paleomagnetic data within the forearc (e.g., Macedo-Sánchez, 1992; Butler et al., 1995; Somoza et al., 1999; Roperch et al., 1999; 2000; Rousse et al., 2005) as well as differential shortening indicate counterclockwise rotation north (up to 45°) of the symmetry axis and clockwise rotation south of it explaining the oroclinal bending of the Andes (Isacks, 1988). This is supported by balanced cross sections (Kley, 1999).

The convergence rate for relative motion between the Nazca plate and South America can be averaged to 7 cm/a (Silver et al., 1998) for the last 30-40 Ma. At the largest width of the orogen between 18-20°S (e.g., Kley, 1999), 280 km of shortening have been accumulated within the last 40 Ma.

The general characteristics of the Andean Altiplano that have been considered as major contributors to the plateau evolution can also be found in our experiments: the compressing piston represents the indenting forearc, our basal detachment simulates a zone of partial melt, which is present beneath the plateau, and the amount of shortening is the same. When comparing the
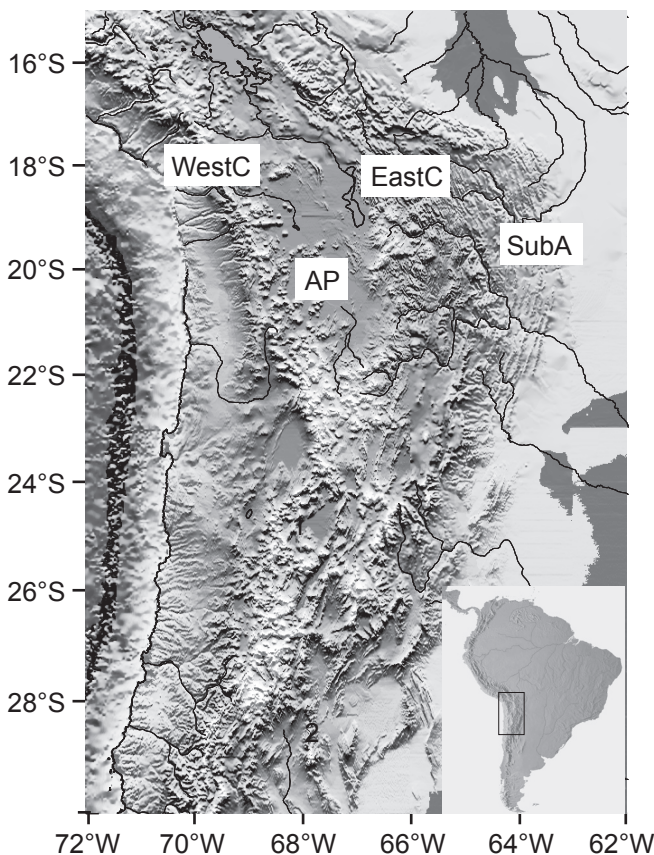


*Fig. 6.6: Topographic map of the Central Andean plateau. The following abbreviations are used: WestC – Western Cordillera, AP – Altiplano, EastC – Eastern Cordillera, SubA – Subandean fold-and-thrust belt.*
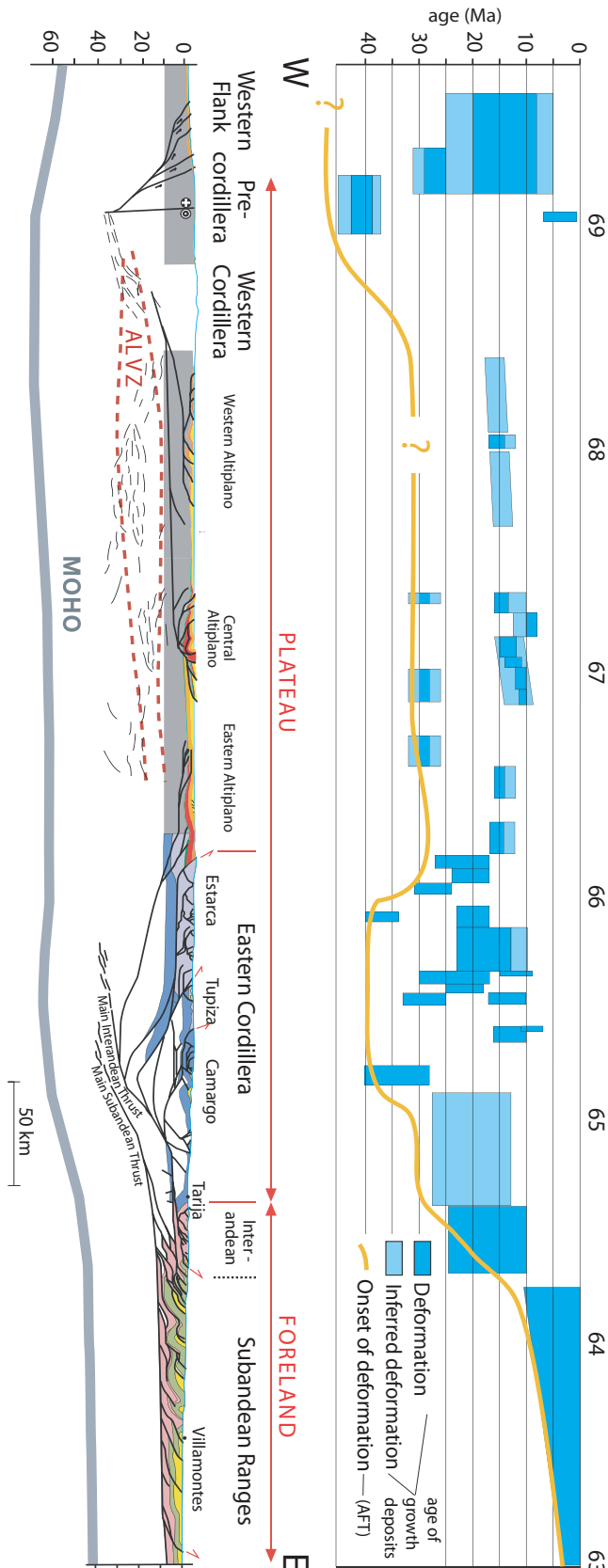
*Fig. 6.7: Top: Deformation timing and duration for each structural unit (from Oncken et al., 2006; data compiled from Gubbels et al., 1993; Kley, 1996; Mueller et al., 2002; Haschke and Guenther, 2003; Silva-Gonzalez, 2004; Victor et al., 2004; Elger et al., 2005; Ege et al., 2007)*
*Bottom: Balanced cross section through the Central Andean Plateau at 21°S (from Oncken et al., 2006; data compiled from Yuan et al., 2000; Mueller et al., 2002; ANCORP-Working Group, 2003; Victor et al., 2004; Elger et al., 2005).*

cross section of our analogue experiments (Fig. 6.4b) with that of the Central Andes at 21°S (Fig. 6.7), we observe that the structural inventory of each of the units is strikingly similar.

Oncken et al. (2006) have attributed the temporal evolution to a special combination of parameters that initiated and controlled the evolution of the Altiplano and the associated strain pattern as well as the amount of strain: feedback of trench infill, plate interface coupling, and associated shortening transfer and slab rollback; changes in relative velocities of trench and upper plate, as well as the position of inherited structures. Certainly we are not able to examine all potential factors that have contributed to the formation of the Central Andes. We also cannot explain why and when the plateau surface has been uplifted to an elevation close to the peak elevation of the Cordilleras, which is still strongly debated (e.g., Gregory-Wodzicki, 2000; Elger, 2003; Garzione et al., 2006; Ghosh et al., 2006; Rech et al., 2006; Eiler et al., 2006).

But we are able to reproduce not only the relative timing of strain accumulation in the Central Andes, but also the spatial deformation pattern. Our Andean-type plateau is solely driven by mechanical heterogeneity and yet shows the same strain partitioning mode as the natural example. The analysis by Oncken et al. (2006) has revealed that only a special combination of driving factors can explain the observed strain pattern. These two very different parameter conditions lead to the formation of a strikingly similar pattern, once in a simple model and in the complex natural example. This means that the strain pattern can be caused by more than one parameter combination and explained by various controlling mechanisms. Therefore, strain patterns should not be used to infer the key controlling factors responsible for the formation of a deformation system.

### 6.7.1. Comparison to other modelling studies

Previous modelling studies on plateau orogens (especially the Central Andean example) mainly focused on the effect of only one parameter: the role of a. thermal perturbation within the lithosphere (Wdowinski and Bock, 1994a; b), b. crustal flow (Royden, 1996), c. gravity-driven channel flow (Husson and Sempere, 2003), d. flow indentation of the lower crust (Gerbault and Willingshofer, 2005), and e. mass flux along a detachment, which caused the formation of the

plateau (Vietor and Oncken, 2005). Only Sobolev and Babeyko (2005) investigated coupled parameters, namely the combined influence of crustal thickness and interplate friction. Certainly, it is highly probable that several parameters in combination affect the formation of a natural system, of which one of the crucial parameters is related to decoupling at the base of the crust.

However, none of these studies was able to explain the spatiotemporal strain pattern as presently observed for a plateau orogen, as most of the studies were not able to reproduce more than a. the final stage of a plateau orogen (Gerbault and Willingshofer, 2005), b. the present-day topography of the Central Andean plateau (Wdowinski and Bock, 1994b; Royden, 1996), or c. the present crustal thickness (Husson and Sempere, 2003).

In contrast, Vietor and Oncken (2005) were already able to reproduce the orogen scale deformation in time and Sobolev and Babeyko (2005) even the timing of topographic development and the approximate amount of shortening over time on the orogen scale. However, being 3D, our study is the first that can reproduce the relative Andean-type distribution of strain accumulation in both space and time on the orogen scale and provides information on the sub-orogen scale as single faults of the structural units are resolved.

Also, we achieve this not only by one single parameter, but we detect the interdependence of two parameters of mechanical heterogeneity. We can pinpoint critical threshold values for these two coupled parameters, which determine the first-order deformational style: wedge- or plateau-like.

### 6.8. Conclusions

In our granular models of the upper crust we can show that a special combination of both basal and lateral strength contrasts determines the style of the resulting deformation system. Depending on critical threshold values for both of these mechanical parameters, either a plateau-style or a wedge-like setting (single- or bivergent) develops. This means that, in the brittle field, the change from one deformation setting to another is not gradual but abrupt, and no transitional deformation types exist in analogue experiments. Being above or below the threshold value exactly determines if either the one setting or the other forms (Fig. 6.2). Finally, we speculate that the deformation modes with distinct thresholds observed in our brittle analogue experiments also pertain to natural orogens exhibiting more complex rheologies.

Our analogue plateau-style settings are able to reproduce a strikingly similar spatial and temporal mode of strain partitioning to the one revealed by the patterns of the Central Andean plateau. Further, we can produce the same strain pattern both on the orogen scale and the sub-orogen scale, although driving factors for the natural example are likely to have been more complex than in our simple models. We conclude that strain patterns are not unique, as various combinations of processes and parameters seem to be able to explain one strain pattern. Therefore, strain patterns should not be used to infer their controlling factors.